Atmos. Chem. Phys., 11, 5539–5555, 2011
www.atmos-chem-phys.net/11/5539/2011/
doi:10.5194/acp-11-5539-2011

Atmospheric Chemistry and Physics

Ice nucleation from aqueous NaCl droplets with and without marine diatoms

P. A. Alpert[1], **J. Y. Aller**[2], **and D. A. Knopf**[1]

[1]Institute for Terrestrial and Planetary Atmospheres/School of Marine and Atmospheric Sciences, Stony Brook University, Stony Brook, NY 11794-5000, USA
[2]School of Marine and Atmospheric Sciences, Stony Brook University, Stony Brook, NY 11794-5000, USA

Received: 20 January 2011 – Published in Atmos. Chem. Phys. Discuss.: 11 March 2011
Revised: 10 May 2011 – Accepted: 1 June 2011 – Published: 16 June 2011

Abstract. Ice formation in the atmosphere by homogeneous and heterogeneous nucleation is one of the least understood processes in cloud microphysics and climate. Here we describe our investigation of the marine environment as a potential source of atmospheric IN by experimentally observing homogeneous ice nucleation from aqueous NaCl droplets and comparing against heterogeneous ice nucleation from aqueous NaCl droplets containing intact and fragmented diatoms. Homogeneous and heterogeneous ice nucleation are studied as a function of temperature and water activity, a_w. Additional analyses are presented on the dependence of diatom surface area and aqueous volume on heterogeneous freezing temperatures, ice nucleation rates, ω_{het}, ice nucleation rate coefficients, J_{het}, and differential and cumulative ice nuclei spectra, $k(T)$ and $K(T)$, respectively. Homogeneous freezing temperatures and corresponding nucleation rate coefficients are in agreement with the water activity based homogeneous ice nucleation theory within experimental and predictive uncertainties. Our results confirm, as predicted by classical nucleation theory, that a stochastic interpretation can be used to describe the homogeneous ice nucleation process. Heterogeneous ice nucleation initiated by intact and fragmented diatoms can be adequately represented by a modified water activity based ice nucleation theory. A horizontal shift in water activity, $\Delta a_{w,het} = 0.2303$, of the ice melting curve can describe median heterogeneous freezing temperatures. Individual freezing temperatures showed no dependence on available diatom surface area and aqueous volume. Determined at median diatom freezing temperatures for a_w from 0.8 to 0.99, $\omega_{het} \simeq 0.11^{+0.06}_{-0.05}\,s^{-1}$, $J_{het} \simeq 1.0^{+1.16}_{-0.61} \times 10^4\,cm^{-2}\,s^{-1}$, and $K \simeq 6.2^{+3.5}_{-4.1} \times 10^4\,cm^{-2}$. The experimentally derived ice nucleation rates and nuclei spectra allow us to estimate ice particle production which we subsequently use for a comparison with observed ice crystal concentrations typically found in cirrus and polar marine mixed-phase clouds. Differences in application of time-dependent and time-independent analyses to predict ice particle production are discussed.

Correspondence to: D. A. Knopf
(daniel.knopf@stonybrook.edu)

1 Introduction

Aerosol particles play an important role in the radiative balance of our Earth's climate by directly scattering and absorbing short wave and long wave radiation (Charlson et al., 1992; Andreae and Crutzen, 1997; Ramanathan et al., 2001; Anderson et al., 2003; McComiskey et al., 2008). They can also act as cloud condensation nuclei (CCN) and ice nuclei (IN) further impacting climate by changing the radiative properties of clouds (Twomey, 1974; Albrecht, 1989; Twomey, 1991; Baker, 1997; Kaufman et al., 2002; Forster et al., 2007; Baker and Peter, 2008). Ice crystals in particular impact atmospheric processes in other ways including the initiation of precipitation with subsequent consequences for the hydrological cycle (Lohmann and Feichter, 2005). Ice can nucleate homogeneously from an aqueous supercooled aerosol particle or heterogeneously by four modes: deposition (the IN nucleates ice directly from the supersaturated vapour phase), immersion (the IN nucleates ice in a supercooled aqueous aerosol particle), condensation (water is taken up by the IN and freezes subsequently), and contact (the impact of an IN with a supercooled aqueous particle nucleates ice) (Vali, 1985; Pruppacher and Klett, 1997).

While it is impossible to directly observe ice nucleation in situ (Hegg and Baker, 2009), heterogeneous ice nucleation is regarded as a possible formation mechanism for cirrus (Heymsfield et al., 1998; DeMott et al., 1998; Seifert et al., 2003; Haag et al., 2003) and mixed-phase clouds (Rogers et al., 2001b; DeMott et al., 2003; Verlinde et al., 2007).

Sea salt particles emitted from oceans constitute the most globally abundant aerosol type by mass. They are important for climate, principally due to their role in the atmosphere as a source for highly reactive halogen species in gas phase, liquid phase, and heterogeneous reactions (Vogt et al., 1996; De Haan et al., 1999; Finlayson-Pitts, 2003; Sander et al., 2003). Sea salt aerosol particles can also act as CCN at low supersaturations with respect to liquid water compared with sulfate particles according to Köhler theory and thus, compete for water vapour in warm clouds despite their relatively low particle concentrations in air (Ghan et al., 1998; O'Dowd et al., 1999; Twohy and Anderson, 2008). Freezing of aqueous sea salt aerosol particles has implications for heterogeneous halogen chemistry and mixed-phase and cirrus cloud formation processes particularly in colder, high-latitude climates. Sea salt residue in cirrus ice crystals were consistently observed from aircraft measurements over the Florida coastline at altitudes around 13 km and indicate the lofting of marine particles by convective systems (Cziczo et al., 2004). Freezing temperatures of micrometer sized aqueous sea salt and NaCl aerosol particles occurs homogeneously below 235 K and follows the water activity based homogeneous ice nucleation theory (Koop et al., 2000b,a). We extend these previous studies to also determine nucleation dependency on a_w, ice nucleation rate coefficients, and the stochastic behavior of the nucleation process. These combined experimental data serve to validate the water activity based ice nucleation theory and aid in explaining in situ observations and model studies of cirrus clouds impacted by marine aerosol particles.

Only a few studies have hinted that marine biogenic particles, i.e. phytoplankton and bacteria, may have the potential to nucleate ice at warmer temperatures than observed for homogeneous freezing (Schnell, 1975; Schnell and Vali, 1976; Fall and Schnell, 1985). Schnell (1975), for example, found efficient IN in laboratory cultures of phytoplankton, however, could not determine if the IN was actually the phytoplankton, their excretory products, associated marine or terrestrial bacteria, or some other nucleating agent. Schnell and Vali (1976) showed that surface sea water contained IN associated with phytoplankton however, they also could not conclusively identify the IN. Fall and Schnell (1985) investigated biogenic ice nucleation using a culture of a marine dinoflagellate species *Heterocapsa niei* which contained a mix of terrestrial and marine bacterial species. A specific bacterium of terrestrial origin found in this mixed culture was isolated and determined to possess an ice active gene, however, they could not identify the actual ice nuclei in the culture (Fall and Schnell, 1985). A study in which the ice nucleating ability of Arctic aerosol particles collected on filter samples was measured, suggested an ocean source of organic ice nuclei, however, no conclusive evidence was provided to specifically identify the organic ice nucleating agent (Rosinski et al., 1986). Finally in a very recent study, several representative Arctic and Antarctic sea-ice bacterial isolates and a polar virus were shown to be very poor IN, nucleating ice at expected homogeneous freezing temperatures (Junge and Swanson, 2008).

A study by Knopf et al. (2010) demonstrated the capability of *Thalassiosira pseudonana*, a marine planktonic diatom with a siliceous cell wall and an organic coating, to act as efficient IN in the immersion mode under typical tropospheric conditions. Here we provide new detailed analysis and discussion on the findings by Knopf et al. (2010) and present new data on homogeneous freezing of aqueous NaCl droplets void of diatoms. In this and the recent Knopf et al. (2010) publication, we focus on diatoms for two reasons. First, they are a diverse group of unicellular marine and freshwater phototrophic organisms which are cosmopolitan in distribution in surface waters and extremely abundant and productive (Stoermer and Smol, 1999). Second, they have been described from atmospheric samples just above sea level and at high altitudes (Darwin, 1846; Brown et al., 1964; Kawai, 1981; Hakansson and Nihlen, 1990). Bigg and Leck (2008) and references therein provide numerous examples of aerosolized diatoms originating from the sea surface microlayer (SML). As a result of aeolian transport, marine diatoms have been found on mountaintops in the Antarctic (Kellogg and Kellogg, 1996; McKay et al., 2008) and as contaminates in snow located in Canada reached by Asian and Arctic air masses (Welch et al., 1991). Diatom fragments identified as amorphous silica at concentrations of 20–28 L^{-1} (air) were collected from ground based sampling at ∼65 m on Amsterdam Island, an isolated volcanic island in the Southern Indian Ocean (Gaudichet et al., 1989). Furthermore, airborne diatom frustules and diatom fragments are ubiquitous in marine Antarctic regions (Chalmers et al., 1996). Diatom fragments have even been shown to accompany African dust plumes in the atmosphere (Harper, 1999), and aircraft measurements at altitudes of over one kilometer have recorded diatoms over continental land masses (Brown et al., 1964).

The fact that diatoms are present in the atmosphere suggests that they may participate in cloud formation processes. While not specifically reporting on the IN efficiency of diatoms, Schnell (1975) and Schnell and Vali (1976) in fact found that regions of greatest atmospheric IN concentrations measured by Bigg (1973) were above major oceanic water mass convergence zones, i.e. the subtropical convergence zone and the Antarctic convergence zone. Characterized by upwelling of nutrient laden bottom waters, overturning, and mixing, these highly productive waters are dominated by diatoms (Alvain et al., 2008).

Periods of high biological activity associated with phytoplankton blooms can produce organic-rich aerosol particles

as a result of bubble bursting and wave breaking processes (O'Dowd et al., 2004; Sciare et al., 2009; Sorooshian et al., 2009; Ovadnevaite et al., 2011). Although most of these studies do not specifically identify aerosolized material, it is well known that a variety of primary biological components including diatoms and other phytoplankters, bacteria, viruses, transparent exopolymers, and colloidal gels are present in the SML and can be aerosolized (Blanchard and Syzdek, 1970; Blanchard, 1975; Aller et al., 2005; Kuznetsova et al., 2005; Bigg and Leck, 2008; Wurl and Holmes, 2008). These biogenic particles may constitute a significant part of the atmospheric aerosol mass fraction in the submicron size range (O'Dowd et al., 2004). A very recent study by Ovadnevaite et al. (2011) reports detection of high contributions of primary organic matter in marine aerosol of $3.8\,\mu g\,m^{-3}$, far greater than organic mass concentrations of on average $1.75\,\mu g\,m^{-3}$ observed in polluted European air masses advected out over the N.E. Atlantic (Dall'Osto et al., 2010; Ovadnevaite et al., 2011). The high organic mass detected by Ovadnevaite et al. (2011) was associated with elevated chlorophyll concentrations in oceanic surface waters, consistent with phytoplankton bloom conditions. A seasonal variability of IN concentrations over the oceans has been observed from filter measurements with the highest concentrations observed in mid-summer and lowest concentrations observed during winter months (Radke et al., 1976; Flyger and Heidam, 1978; Borys, 1983; Bigg, 1996). The mixed-phase Arctic cloud experiment (M-PACE) reports a mean IN concentration of $\simeq 0.8\,L^{-1}$ (air) in fall using a continuous flow diffusion chamber (CFDC) (Verlinde et al., 2007; Prenni et al., 2009). Springtime IN concentrations in the Arctic measured during the NASA FIRE Arctic Cloud Experiment (ACE) and Surface Heat Budget of the Arctic (SHEBA) program (Rogers et al., 2001a) were enhanced by a factor of 5 ($\sim 4\,L^{-1}$ (air)) over those measured during fall months (Prenni et al., 2009). Using similar IN measurement techniques and air mass trajectory analysis, periods of elevated primary production in surface waters could be related to observed IN concentrations (Bigg, 1996; Rogers et al., 2001a; Prenni et al., 2009).

Here we present a comparative analysis of homogeneous and heterogeneous freezing of aqueous NaCl droplets with and without intact and fragmented marine diatoms, for the remainder of the manuscript referred to as aqueous NaCl/diatom droplets and aqueous NaCl droplets, respectively. We investigated homogeneous freezing of aqueous NaCl droplets with respect to the water activity based homogeneous ice nucleation theory (Koop et al., 2000b). We use optical microscopy to individually observe thousands of aqueous NaCl droplet freezing temperatures (Koop et al., 1998; Knopf and Lopez, 2009; Knopf and Rigg, 2011). Optical microscopy also allows for direct measurements of individual droplet volume, and thus experimental determination of homogeneous ice nucleation rate coefficients of micrometer sized aqueous NaCl droplets. We examined heterogeneous freezing of diatoms via the immersion mode with respect to the modified water activity based ice nucleation theory (Zobrist et al., 2008; Koop and Zobrist, 2009). We also determined diatom surface area and aqueous volume dependence on heterogeneous freezing temperatures. Additionally, we quantify heterogeneous ice nucleation from intact and fragmented diatoms immersed in droplets in terms of time-dependent and time-independent approaches. A time-dependent analysis is used to derive heterogeneous ice nucleation rates and a time-independent analysis to derive ice active surface site densities, both of which allow for estimations of atmospheric ice particle production. The atmospheric implications of our findings are discussed.

2 Experiment

2.1 Diatom characteristics and preparation

Preparation of *T. pseudonana* for ice nucleation experiments briefly described in Knopf et al. (2010) are more thoroughly described below. Diatoms were grown under axenic conditions in unialgal, clonal cultures in 0.2 µm filtered, autoclaved seawater with F/2 nutrient supplement (Guillard, 1962) commonly used to grow diatoms (Fisher and Wente, 1993) at temperatures from 16 °C to 18 °C and a 14 h light/10 h dark cycle. Cells were harvested after one week when concentrations reached $\sim 10^6$ cells mL^{-1}. Microscopic inspection allowed determination of cell concentrations and to affirm that the diatom cultures remained axenic at every step in the preparation, conditioning, and ice nucleation experiments. Small samples of cultures ($\sim$0.1 mL) were stained with acridine orange, a nucleic acid fluorescent dye, and counted utilizing epifluorescence microscopy (Hobbie et al., 1977; Watson et al., 1977). Prior to application in our experiments, *T. pseudonana* were washed with a 3.5 wt % aqueous NaCl solution made up using millipore water (resistivity $>18.2\,M\Omega\,cm$). Diatom cells were added to a second aqueous NaCl solution for droplet generation concentrated to $\sim 3\times 10^7$ cells mL^{-1}. These final solutions were either used immediately to generate droplets as described below or stored for subsequent use at 5 °C for no longer than 24 h. The potential for silica dissolution to impact the surface properties of diatoms was negligible during this storage period given the large mass of diatoms in suspension, which was more than two orders of magnitude greater than the soluble mass of SiO_2.

2.2 Aerosol particle generation

Homogeneous and heterogeneous ice nucleation were observed on 5000 individually generated aqueous aerosol particles in more than 50 separate experiments employing a novel experimental ice nucleation setup (Knopf and Lopez, 2009). Heterogeneous and homogeneous ice nucleation were determined from aqueous NaCl droplets with and without diatoms

and/or diatom fragments immersed inside. Monodispersed aqueous aerosol particles were generated using a piezoelectric driven single drop dispenser. Average droplet diameters ranged from 40–70 µm. 30–50 droplets per sample were deposited in a gridded pattern on a hydrophobically coated glass slide which served as the base plate of the aerosol cell as described below (Koop et al., 1998; Knopf et al., 2002, 2003; Knopf, 2006; Knopf and Lopez, 2009; Knopf and Rigg, 2011). Aerosol generation was conducted in a laminar flow clean bench to avoid contamination by ambient particles (Knopf and Lopez, 2009).

2.3 Diatom surface area

Direct measurements of diatom surface areas were made for each aqueous NaCl/diatom droplet. Once a freezing experiment was completed, the number of intact diatoms and fragments of diatoms immersed in an aqueous NaCl/diatom droplet were determined using an optical microscope at 500× magnification with transmitted light and polarizing filters. The average geometric diatom surface area was estimated using SEM images to be $\sim 1.2\times10^{-6}\,\mathrm{cm}^2$ corresponding to a size of roughly 5 µm in diameter. Cell fragments were estimated to be an order of magnitude smaller in surface area than whole diatom cells although this may represent a lower limit of the actual surface area. The total surface area contributed by diatoms inside each aqueous NaCl/diatom droplet was then calculated by summing the number of immersed diatom cells and fragments and corresponding SEM derived surface areas. The vast majority of droplets contained whole cells and cell fragments, with only 1 % of the droplets examined containing only fragments. The log-normal distribution of diatom cells immersed in aqueous NaCl/diatom droplets (not shown) had a mode of 3 cells per droplet. 90 % of all investigated aqueous NaCl/diatom droplets contained fewer than 25 diatom cells per droplet and only 5 % of the droplets contained more than 37 whole cells.

2.4 Aerosol particle conditioning

Promptly after particle generation, aqueous NaCl or aqueous NaCl/diatom droplets were placed inside an aerosol conditioning cell (ACC) (Knopf and Lopez, 2009; Knopf and Rigg, 2011). The temperature of the droplets, T_d, was controlled using a home made cryo-cooling stage coupled to an optical microscope (Knopf and Lopez, 2009). The ACC was purged with a controlled humidified N_2 gas flow with a constant dew point, T_dew. The water partial pressure was derived from the measured T_dew (Knopf and Lopez, 2009) with an accuracy of ±0.15 K. The relative humidity (RH) experienced by the droplets in the ACC was controlled by adjusting T_d at constant T_dew. T_d was in the range of 291–296 K depending on the desired RH. Calibration of the ACC was performed according to Knopf and Lopez (2009) by measuring the melting temperature of ice particles and deliquescence relative humidity of NaCl, $(NH_4)_2SO_4$, LiCl and K_2SO_4 particles, resulting in an uncertainty of less than ±0.1 K.

The conditioning procedure was as follows. Inside the ACC, droplets were exposed to a specific RH and allowed to reach equilibrium with the water vapour (Knopf and Lopez, 2009). For an aqueous solution in equilibrium with water vapour, RH is equal to water activity, a_w (Koop et al., 2000b). The error in a_w was ±0.01 due to the uncertainty in T_dew and T_d. Subsequently, the droplets inside the aerosol cell were sealed against ambient air with a cover slide and a greased aluminum foil spacer (Koop et al., 1998; Knopf and Lopez, 2009). The dimensions of the aerosol cell were designed in such a way that the number of water molecules in the gas-phase were negligible compared to the condensed-phase water so that upon cooling of the droplets, no changes in droplet composition from water condensation resulted (Koop et al., 1998; Knopf and Lopez, 2009).

2.5 Ice nucleation experiments

The aerosol cell was transferred from the ACC to a second cryo-cooling stage attached to an optical microscope to observe freezing and melting of droplets as described by Knopf and Lopez (2009). Temperature calibration of this cryo-stage was performed by measuring the melting temperatures of heptane (182.60 K), octane (216.33 K), decane (243.55 K), dodecane (263.58 K), and ice (273.15 K) (Knopf et al., 2002, 2003; Knopf and Lopez, 2009). The temperature sensor for the stage indicated a linear temperature change for the range of 170–280 K to within less than 0.1 K. The droplets were cooled at a rate of $10\,\mathrm{K\,min}^{-1}$ until all of the droplets in the aerosol cell froze. The cooling rate was rapid enough to avoid effects from mass transport of water vapour from liquid to ice particles, but not so fast as to significantly lower freezing temperatures (Koop et al., 1998; Bertram et al., 2000; Knopf and Lopez, 2009). The heating rate to observe melting of ice was $0.5\,\mathrm{K\,min}^{-1}$. For each aerosol sample, freezing and melting was observed for a maximum of 3 repetitions. A digital camera with imaging software recorded freezing and melting temperatures in addition to measurements of droplet diameter and the number of cells per droplet on a hard drive for subsequent analysis. Droplet diameters were corrected for non-sphericity.

3 Results and discussion

3.1 Homogeneous freezing of aqueous NaCl droplets

Figure 1 summarizes melting and homogeneous freezing of about 2500 aqueous NaCl droplets as a function of temperature, T, and wt % and a_w determined at particle preparation conditions. The corresponding raw data is shown in Fig. 2 and will be discussed below. Direct measurements of a_w for aqueous NaCl droplets in the supercooled temperature regime do not exist (Koop, 2004), and thermodynamic

Table 1. Summary of ice nucleation parameters evaluated at median freezing temperatures for homogeneous and heterogeneous ice nucleation given in the top and bottom panel, respectively. Median heterogeneous freezing and mean melting temperatures of intact and fragmented diatoms were taken from Knopf et al. (2011). All other values were obtained from this study.

a_w	0.984	0.970	0.953	0.924	0.900	0.874	0.851	0.826	0.806
T_f^{NaCl} K	232.8	230.6	228.5	222.5	216.4	212.6	209.8	203.5	200.5
$T_f^{Koop}(a_w)$ K	233.9	231.6	228.7	223.2	217.9	211.3	204.3	195.9	188.9
T_m^{NaCl} K	271.6	270.3	268.6	265.8	261.5	259.6	257.3	254.6	252.6
$S_{ice}(T_f^{NaCl})$	1.45	1.46	1.46	1.50	1.51	1.51	1.50	1.51	1.50
$J_{hom}(T_f^{NaCl})\times10^6$ cm^{-3} s^{-1}	3.52	2.07	1.00	1.66	1.40	2.56	1.26	3.31	0.44
a_w	0.984	0.969	0.951	0.926	0.902	0.873	0.850	0.826	0.800
T_f^{dia} K	242.3	241.1	238.6	234.0	232.0	224.9	224.7	220.7	216.6
T_m^{dia} K	271.6	270.5	268.7	265.7	263.5	259.3	257.3	254.5	253.9
$S_{ice}(T_f^{dia})$	1.33	1.32	1.33	1.35	1.34	1.38	1.35	1.35	1.35
$\omega_{het}(T_f^{dia})$ s^{-1}	0.13	0.17	0.13	0.11	0.11	0.06	0.13	0.07	0.08
$J_{het}(T_f^{dia})\times10^4$ cm^{-2} s^{-1}	1.51	0.44	1.50	0.39	0.70	0.64	2.16	0.75	1.14
$k(T_f^{dia})\times10^4$ cm^{-2} K^{-1}	7.5	2.3	8.7	2.6	2.2	2.0	6.0	5.1	9.5
$K(T_f^{dia})\times10^4$ cm^{-2}	9.1	2.1	6.4	2.9	3.0	7.7	8.3	7.0	9.7

models for aqueous NaCl only provide a_w for a range of concentrations at 298.15 K (Clegg et al., 1998), thus we assume that aqueous droplet a_w determined at the preparation conditions does not change with decreasing T (Koop et al., 2000a,b). The ice melting curve, $a_w^{ice}(T)$, is the activity of water in solution in equilibrium with ice (Koop et al., 2000b; Koop and Zobrist, 2009). Within our experimental uncertainty, Fig. 1 indicates good agreement of our experimentally determined mean melting temperatures, T_m^{NaCl}, with $a_w^{ice}(T)$ (Koop et al., 2000b; Murphy and Koop, 2005; Koop and Zobrist, 2009). Within experimental and theoretical uncertainties, our experimentally derived median homogenous freezing temperatures, T_f^{NaCl}, are in good agreement with predicted freezing temperatures. The predicted homogeneous freezing curve was adjusted for the droplet diameters employed in our experiments (Koop et al., 2000b; Koop and Zobrist, 2009). T_f^{NaCl} for a_w of 0.806 shows slightly warmer temperatures than predictions. This may be explained by the formation of $NaCl{\cdot}2H_2O$ (Koop et al., 2000a) which may have affected the freezing process. The melting of all crystalline particles prepared at $a_w = 0.806$ was visually different to the melting of crystalline particles prepared at higher a_w. The observed melting temperature at $a_w = 0.806$ may indicate the melting of the eutectic mixture at the temperature of 252 K (Koop et al., 2000a). Another explanation for the slight deviations of T_f^{NaCl} from the homogeneous freezing curve at low a_w may be that a_w does change in the supercooled region, particularly for highly concentrated NaCl solutions. Freezing and melting temperatures shown in Fig. 1 for the investigated a_w are given in Table 1, in addition to corresponding ice saturation ratios evaluated at median freezing temperatures, $S_{ice}(T_f^{NaCl})$, and predicted freezing temperatures, $T_f^{Koop}(a_w)$. The data displayed in Fig. 1 indicates that the variations in the melting temperatures are smaller than for the corresponding freezing temperatures. This is primarily due to the stochastic nature of the ice nucleation process, although, the presence of different droplet sizes and possible events of heterogeneous ice nucleation could contribute to the difference (Koop et al., 1998; Knopf and Lopez, 2009; Knopf and Rigg, 2011).

Figure 2 summarizes all observed ice nucleation events from aqueous NaCl droplets, where each panel corresponds to a different a_w value at particle preparation conditions. The frozen fraction of droplets, f, was calculated from observations by $f = N_{ice}/N_{tot}$, where N_{ice} is the number of frozen particles as a function of T, and N_{tot} is the total number of analyzed droplets. These data points manifest a cumulative distribution as a function of T. The uncertainty of f indicates the range within a temperature increment of 0.2 K. The probability density histogram (PDH) binned in 1.0 K increments was normalized to N_{tot} with the increment size chosen to better visualize the distribution of freezing frequencies.

We applied a normal distribution to describe the stochastic nature of homogeneous ice nucleation and thus f (Koop et al., 1997; Pruppacher and Klett, 1997). As discussed previously in detail, the probability of observing n nucleation events from the binomial distribution is approximated by the Poisson distribution using Stirling's formula under typical conditions for homogeneous nucleation of aqueous aerosol particles (Koop et al., 1997). If a large number of nucleation events are observed, $n>100$, then the binomial distribution reduces to a normal distribution (Ross, 1996; Koop et al., 1997).

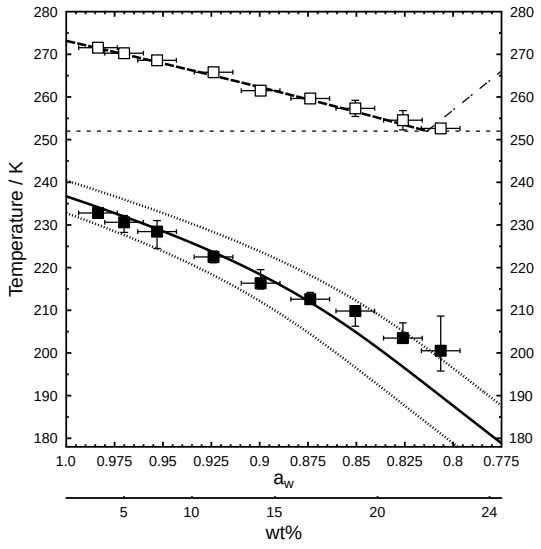

Fig. 1. Median homogeneous freezing temperatures and corresponding mean melting temperatures for aqueous NaCl droplets are shown as filled and open squares, respectively, as a function of a_w and wt %. The error bars for the freezing temperatures indicate the 10th and 90th percentile and error bars for the melting temperatures indicate one standard deviation. Uncertainty in a_w is ± 0.01. The narrow dashed line represents the ice melting curve (Koop and Zobrist, 2009). The wide dashed line and the dash-dotted lines indicate the eutectic temperature and the solid-liquid equilibrium curve of $NaCl{\cdot}2H_2O$, respectively (Linke, 1965; Clarke and Glew, 1985). The solid line represents the predicted homogeneous freezing curve (Koop and Zobrist, 2009). The two dotted lines represent an uncertainty of the homogeneous freezing curve due to an uncertainty in a_w of ± 0.025 (Koop, 2004). It is assumed that a_w of the aqueous droplets does not change with temperature (Koop et al., 2000b,a).

The red solid curve in Fig. 2 is a fit of f to a normal cumulative distribution function (CDF) according to

$$f_{\text{fit}} = \frac{1}{2}\left[1 - \text{erf}\left(\frac{T-\mu}{\sqrt{2}\sigma}\right)\right] \quad (1)$$

where μ and σ are the mean and standard deviation fitting parameters that describe the distribution. Figure 2 indicates that our observed freezing events are in very good agreement with Eq. (1). Deviations of observed ice nucleation distributions from f_{fit} were mostly found at higher temperatures due to possible heterogeneous freezing events. However, the number of heterogeneous ice nucleation events were too few compared with N_{tot} to provide any significant weighting to the fit. Deviations of observed ice nucleation distributions from the fits for lower temperatures occur for aqueous NaCl droplets with lowest a_w of 0.806–0.851. This is likely due to our experimental uncertainty a_w. In an analysis (not shown here) in which only the data within the 10th and 90th percentiles were employed to obtain f_{fit}, corresponding values for μ and σ were found not to be affected significantly. Again this was due to the larger number of homogeneous ice nucleation events that occurred compared to the few heterogeneous ice nucleation events.

Here, we derive homogeneous ice nucleation rate coefficients, J_{hom}, for aqueous NaCl droplets with varying initial a_w. The analytical approach and corresponding interpretation of J_{hom} has been explained in detail previously (Koop et al., 1997; Zobrist et al., 2007). In a chosen temperature interval, ΔT, different numbers of freezing events will occur. We derived $J_{\text{hom}}(T^i)$ as the average homogeneous ice nucleation rate coefficient at the mean temperature, T^i, of the i-th temperature interval. This derivation employed all experimental data, including the data points outside of the 10th and 90th percentiles, using the following formula,

$$J_{\text{hom}}(T^i) = \frac{n^i_{\text{nuc}}}{t^i_{\text{tot}} \cdot V^i}, \quad (2)$$

where n^i_{nuc} is the number of nucleation events that occur within the i-th temperature interval, t^i_{tot} is the total observation time in the i-th temperature interval, and V^i accounts for the individual droplet volumes available at the start of the temperature interval, T^i_{st}, those of which remain liquid throughout the i-th interval and those which freeze within this interval. The product $t^i_{\text{tot}} \cdot V^i$ is given by the sum of the contribution from the droplets that remain liquid and those that freeze according to

$$t^i_{\text{tot}} \cdot V^i = \frac{\Delta T}{r} V^i_{\text{liq}} + \sum_{j=1}^{n^i_{\text{nuc}}} \frac{1}{r}\left(T^i_{\text{st}} - T^i_{\text{nuc},j}\right) V^i_{\text{liq},j}, \quad (3)$$

where r is the experimental cooling rate, V^i_{liq} is the total volume that remains liquid until the end of the temperature interval, and $T^i_{\text{nuc},j}$ and $V^i_{\text{liq},j}$ are the freezing temperature and corresponding volume, respectively, of the j-th droplet nucleating ice within the i-th interval. Derivations of $J_{\text{hom}}(T^i)$ employ $\Delta T = 0.2$ K corresponding to our total experimental error in determining the temperature. As discussed above, experimental heterogeneous ice nucleation events cannot be avoided when studying homogeneous nucleation (Knopf and Lopez, 2009), however, this effect is not critical for deriving J_{hom} as a function of T due to the goodness of the fit in Fig. 2 and the insignificant number of heterogeneous compared to homogeneous freezing events as previously discussed.

Figure 3 shows experimentally derived J_{hom} as a function of T and initial a_w. J_{hom} values for given a_w which extend to higher temperatures and do not show a strong increase with decreasing temperature, are most likely affected by heterogeneous freezing events. For example, the freezing data for aqueous NaCl droplets with $a_w = 0.900$ in Fig. 3 does not show a strong increase in J_{hom} for temperatures between 220–226 K, and remain almost constant at values below $10^5\,\text{cm}^{-3}\text{s}^{-1}$. However, J_{hom} values increase significantly from 220 K to 214 K as the homogeneous freezing limit is approached. Also shown in Fig. 3 are theoretical predictions of J_{hom} applying the water-activity based homogeneous ice nucleation theory, $J^{\text{Koop}}_{\text{hom}}$, for each initial a_w (Koop

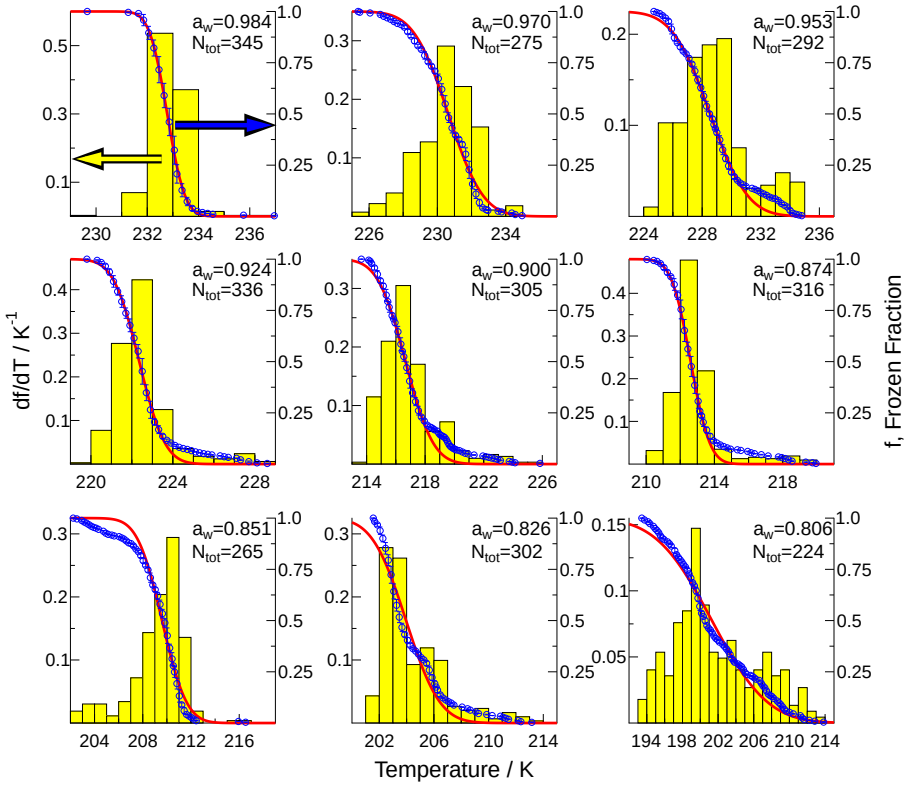

Fig. 2. Summary of all observed homogeneous ice nucleation events as a function of a_w and T. The frozen fraction, f, of droplets in 0.2 K temperature increments is represented by blue circles. Error bars indicate the range of f in a temperature increment of 0.2 K. Yellow bars show the probability density histogram (PDH) binned in 1.0 K increments. For each panel, a_w and the total number of analyzed droplets, N_{tot}, are given. The values for the PDH are given on the left y-axis and f on the right y-axis.

et al., 2000b; Koop and Zobrist, 2009). Within the theoretical uncertainty, J_{hom}^{Koop} agrees with the experimental data. A potential exception are J_{hom} values obtained for $a_w = 0.806$ for which J_{hom}^{Koop} under predicts our observations. This may be due to the occurrence of heterogeneous ice nucleation events and/or the unknown behavior of supercooled aqueous NaCl solutions, especially at this low a_w value. It should be noted that the uncertainty of the a_w based homogeneous ice nucleation theory for $a_w = 0.800$, is given as ± 0.05 in a_w which translates to ± 12 orders of magnitude uncertainty in predictions of J_{hom} (Koop, 2004). J_{hom} evaluated at T_f^{NaCl} given in Table 1 remains the same to within one order of magnitude. This translates into a corresponding constant shift in water activity, Δa_w, as suggested by the water-activity based homogeneous ice nucleation theory (Koop et al., 2000b). Deviations between the observed and predicted J_{hom} values for aqueous NaCl droplets may be attributed to the unknown behavior of a_w in the supercooled temperature regime (Knopf and Rigg, 2011). The J_{hom} presented here can be employed to further constrain the water-activity based homogeneous ice nucleation theory (Koop et al., 2000b; Knopf and Lopez, 2009; Knopf and Rigg, 2011).

3.2 Heterogeneous freezing of aqueous NaCl droplets containing diatoms

Median heterogeneous freezing temperatures of aqueous NaCl droplets containing diatoms *T. pseudonana*, T_f^{dia}, and corresponding mean melting temperatures, T_m^{dia}, are shown in Fig. 4 as a function of a_w and droplet composition (Knopf et al., 2010). The droplet composition was calculated using the E-AIM model (Clegg et al., 1998) and assuming that a_w remains constant with temperature. Within the experimental uncertainty T_m^{dia} are in good agreement with $a_w^{ice}(T)$ (Koop et al., 2000b; Koop and Zobrist, 2009). The homogeneous freezing curve (Koop et al., 2000b; Koop and Zobrist, 2009) is plotted for comparison. Clearly, freezing occurs at much higher temperatures for aqueous NaCl/diatom droplets (Knopf et al., 2010) compared to predicted homogeneous ice nucleation temperatures. At high a_w, corresponding to more dilute solutions, ice nucleation temperatures are enhanced by $\sim$10 K compared to the homogeneous freezing temperatures. At low a_w, ice nucleation proceeds at temperatures $\sim$30 K above predicted homogeneous freezing temperatures. T_m^{dia} and T_f^{dia} shown in Fig. 4 for the investigated a_w are given in Table 1, in addition to $S_{ice}(T_f^{dia})$.

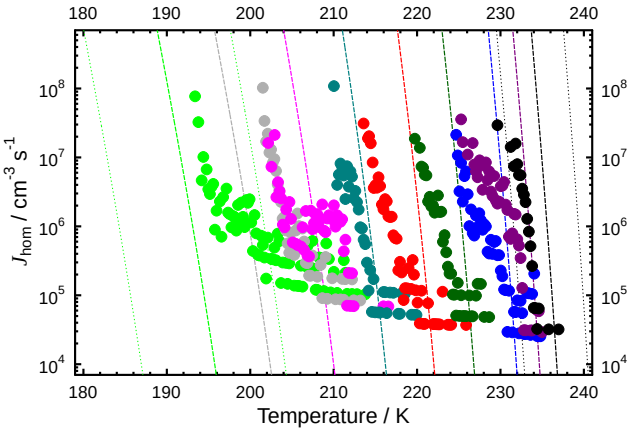

Fig. 3. Experimentally derived homogeneous ice nucleation rate coefficients, J_{hom} (circles), and theoretically predicted J_{hom} values (dashed lines) (Koop et al., 2000b) shown as a function of T and a_{w}. Black, purple, blue, green, red, teal, magenta, gray, and lime colors correspond to aqueous NaCl droplets with initial a_{w} of 0.984, 0.970, 0.953, 0.924, 0.900, 0.874, 0.851, 0.826, 0.806. The uncertainty for predicted J_{hom} due to an uncertainty in a_{w} of ± 0.025 is indicated as dotted lines for a_{w} of 0.984 and 0.806.

The experiments above were repeated using the same aqueous diatom solution, but filtered using a 0.1 µm filter to remove diatoms and possible fragments. This procedure resulted only in homogeneous ice nucleation indicating that the diatoms cause heterogeneous ice nucleation in the immersion mode at elevated temperatures and not dissolved organic material associated with the diatom.

Previous work suggests that heterogeneous immersion mode nucleation can be described by a horizontal shift of the ice melting curve, $\Delta a_{\mathrm{w,het}}$, similar to the derivation of homogeneous ice nucleation temperatures (Koop et al., 2000b; Koop and Zobrist, 2009). Following this approach, we derive a heterogeneous freezing curve given by

$$a_{\mathrm{w}}^{\mathrm{f,het}}(T) = a_{\mathrm{w}}^{\mathrm{ice}}(T) + \Delta a_{\mathrm{w,het}}. \quad (4)$$

The new freezing curve, $a_{\mathrm{w}}^{\mathrm{f,het}}(T)$, was constructed by fitting $T_{\mathrm{f}}^{\mathrm{dia}}$ to Eq. (4) leaving $\Delta a_{\mathrm{w,het}}$ as the only free parameter. The best fit yields $\Delta a_{\mathrm{w,het}} = 0.2303$ to describe $T_{\mathrm{f}}^{\mathrm{dia}}$. The data presented in Fig. 4 indicates that $T_{\mathrm{f}}^{\mathrm{dia}}$ is in good agreement with the modified water-activity based ice nucleation theory for predictions of heterogeneous immersion freezing if similar uncertainties as made for predictions of homogeneous freezing are assumed (Koop, 2004). For $a_{\mathrm{w}} < 0.85$, $T_{\mathrm{f}}^{\mathrm{dia}}$ show a slight trend to higher freezing temperatures compared to the predictions. Nevertheless, the overall good agreement of $T_{\mathrm{f}}^{\mathrm{dia}}$ with $a_{\mathrm{w}}^{\mathrm{f,het}}(T)$ described by $\Delta a_{\mathrm{w,het}}$ indicates that heterogeneous ice nucleation induced by intact and fragmented diatoms can be adequately described by thermodynamic quantities (Zobrist et al., 2008; Koop and Zobrist, 2009).

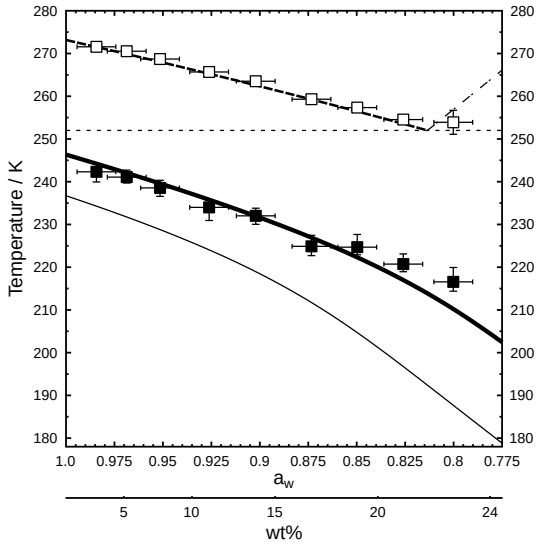

Fig. 4. Median freezing temperatures and mean melting temperatures of aqueous NaCl/diatom droplets are shown as filled and open squares, respectively as a function of a_{w} and wt %. The uncertainty for the freezing temperatures are given by the 10th and 90th percentiles and the uncertainty in the melting temperature represents one standard deviation. The error in a_{w} is ± 0.01. The thick solid line represents the ice melting curve shifted by $\Delta a_{\mathrm{w,het}} = 0.2303$, and the thin solid line is the homogeneous freezing curve (Koop and Zobrist, 2009). Other lines are the same as in Fig. 1.

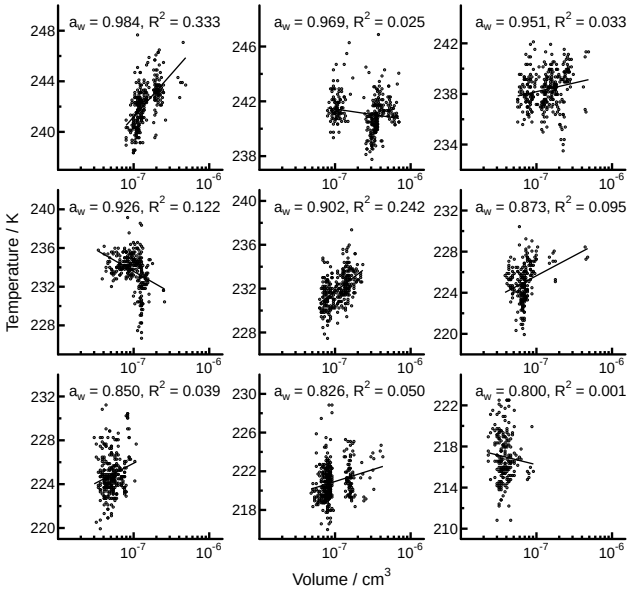

Fig. 5. Heterogeneous freezing temperatures of aqueous NaCl/diatom droplets shown as dots are plotted as a function of droplet volume for each investigated water activity. The solid lines represent best fits to the data. The coefficient of determination, R^2, indicates the quality of the corresponding fits.

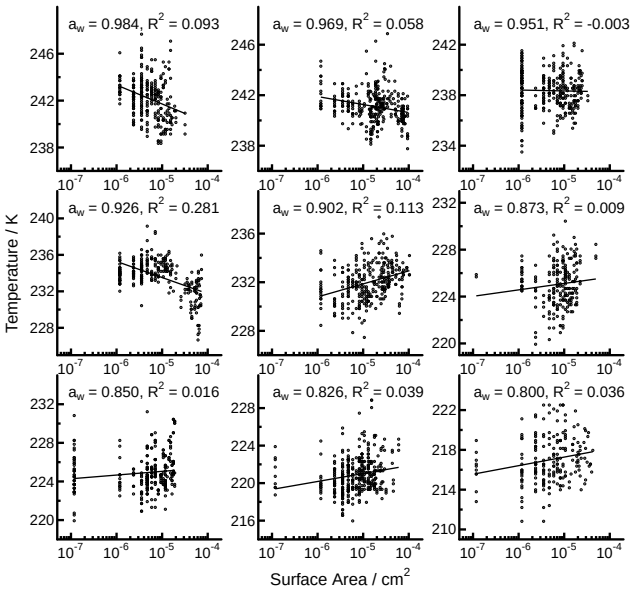

Fig. 6. Heterogeneous freezing temperatures of aqueous NaCl/diatom droplets shown as dots are plotted as a function of diatom surface area for each investigated water activity. The solid lines represent best fits to the data. The coefficient of determination, R^2, indicates the quality of the corresponding fits.

Figure 5 shows all observed heterogeneous freezing temperatures from Fig. 4 as a function of aqueous NaCl/diatom droplet volume and a_w. A linear fit to the data in Fig. 5 indicates for the most part no or very weak correlations between observed freezing temperatures and droplet volume as determined from given R^2 coefficients (R^2<0.2) except for $a_w = 0.984$ and 0.902. Over the experimentally accessed range of volumes and a_w the freezing temperatures do not depend significantly on the volume of the droplet.

Figure 6 shows the heterogeneous freezing temperatures of aqueous NaCl/diatom droplets as a function of estimated diatom surface area for all investigated a_w. Similar to Fig. 5, linear fits to the data and corresponding R^2 coefficients were determined. The R^2 coefficients indicate that there is no correlation between diatom surface area and freezing temperature except very weak correlation for droplets with initial a_w of 0.926. In summary, the surface area dependence was less than the scatter in the data which was approximately 4–6 K.

Figure 7 summarizes approximately 2500 observed heterogeneous ice nucleation events as a function of T and a_w. The cumulative distribution and f in addition to the PDH for heterogeneous freezing, were determined as described above for homogeneous ice nucleation of aqueous NaCl droplets. The PDH and cumulative distributions for heterogeneous ice nucleation due to diatoms immersed in aqueous NaCl droplets show striking similarities to the ones derived from homogeneous nucleation of aqueous NaCl droplets without diatoms shown in Fig. 2.

To quantify the heterogeneous freezing behavior of diatoms via the immersion mode, we consider two analytical approaches, a time-dependent (Bigg, 1953) and a time-independent (Dorsey, 1948). The time-dependent approach follows classical nucleation theory which maintains that heterogeneous ice nucleation, like homogeneous ice nucleation, is dominated by molecular kinetics. Water molecules in an aqueous phase randomly cluster and break apart on the surface of an IN, and each cluster that forms has a probability of growing large enough in time to become the center of a critical ice embryo and subsequently trigger bulk phase ice nucleation (see e.g. Pruppacher and Klett, 1997). The time-independent approach maintains that the dominant influence of heterogeneous nucleation is the presence of surface inhomogeneities which act as preferred sites, or "active sites", of critical ice embryo formation and thus, ice nucleation (Vali, 1971, 1994; Pruppacher and Klett, 1997). These active sites are then destined to become IN at site-specific characteristic temperatures. Thus, ice nucleation is triggered by the appearance of active sites as a function of temperature on the surface of particles immersed in aqueous droplets (Vali, 1971).

3.2.1 Time-dependent analysis

Here, we quantify heterogeneous ice nucleation due to intact and fragmented diatoms employing a time-dependent approach. As indicated in Fig. 6, heterogeneous freezing temperature dependence on diatom surface area was less than the scatter in the data. We therefore derive heterogeneous ice nucleation rates independent of diatom surface area as a function of T and a_w. However, in the case where ice nucleation is found to depend on diatom surface area outside the range probed in our experiments and/or diatom surface areas are available from field samples, we additionally provide surface dependent heterogeneous ice nucleation rate coefficients as a function of T and a_w.

We follow a previously described analysis (Koop et al., 1997; Zobrist et al., 2007) to calculate the time-dependent heterogeneous ice nucleation rate given as

$$\omega_{het}(T^i) = \frac{n^i_{nuc}}{t^i_{tot}}, \quad (5)$$

and t^i_{tot} is given by

$$t^i_{tot} = \frac{\Delta T}{r}\left(n^i_{tot} - n^i_{nuc}\right) + \sum_{j=1}^{n^i_{nuc}} \frac{1}{r}\left(T^i_{st} - T^i_{nuc,j}\right), \quad (6)$$

where n^i_{tot} is the total number of liquid droplets at the start of the i-th temperature interval. The remaining variables are the same as in Eq. (3).

Measurements of diatom surface area and observations of heterogeneous freezing events allowed us to derive heterogeneous ice nucleation rate coefficients, J_{het}. Following a previously described analysis (Koop et al., 1997; Zobrist et al.,

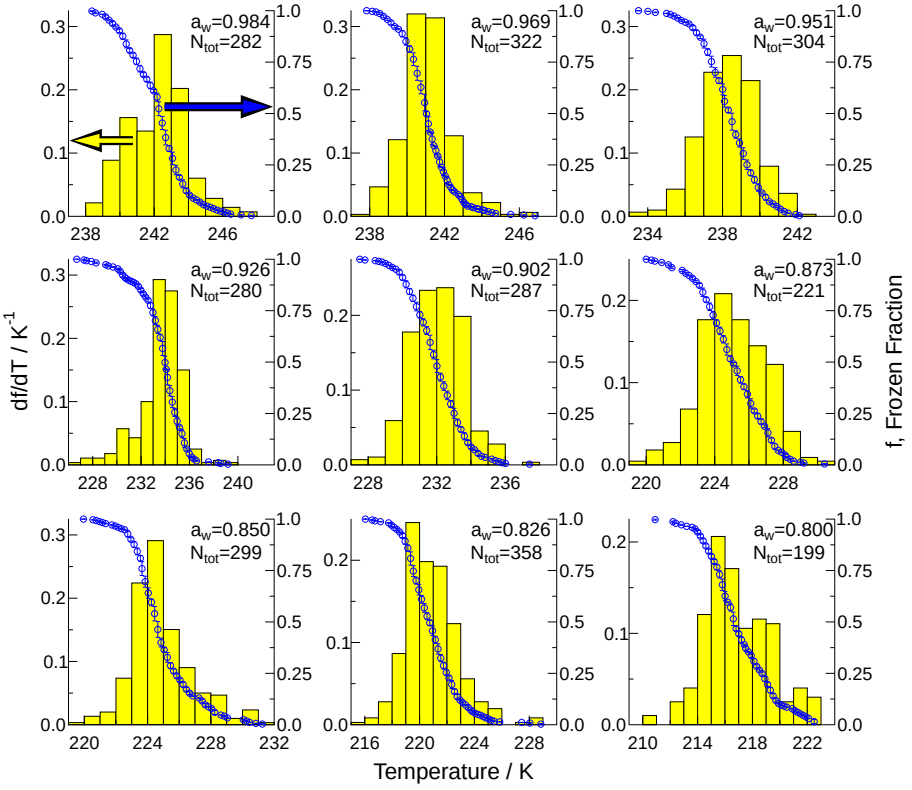

Fig. 7. Summary of all observed heterogeneous ice nucleation events as a function of a_w and T. The frozen fraction, f, of droplets in 0.2 K temperature increments is represented by blue circles. Error bars indicate the range of f in a temperature increment of 0.2 K. Yellow bars show the probability density histogram (PDH) binned in 1.0 K increments. For each panel, a_w and the total number of analyzed droplets, N_{tot}, are given. The values for the PDH are given on the left y-axis and f on the right y-axis.

2007), $J_{het}(T^i)$ is the average heterogeneous ice nucleation rate coefficient for a given temperature interval which can be described as

$$J_{het}(T^i) = \frac{n^i_{nuc}}{t^i_{tot} \cdot A^i}. \quad (7)$$

The product $t^i_{tot} \cdot A^i$ is derived according to

$$t^i_{tot} \cdot A^i = \frac{\Delta T}{r} A^i_{liq} + \sum_{j=1}^{n^i_{nuc}} \frac{1}{r} \left(T^i_{st} - T^i_{nuc,j} \right) A^i_{liq,j}. \quad (8)$$

A^i_{liq} is the total diatom surface area in the droplets that remains liquid until the end of the temperature interval and $A^i_{liq,j}$ is the diatom surface area of the j-th droplet that nucleates ice within the i-th temperature interval. Other variables are the same as in Eqs. (3) and (6). For calculation of $\omega_{het}(T)$ and $J_{het}(T)$, $\Delta T = 0.2$ K reflects the experimental temperature uncertainty.

Figure 8a, b presents ω_{het} and J_{het}, respectively, for the individually analyzed ice nucleation events presented in Fig. 7 as a function of T and a_w. Figure 8 demonstrates that ω_{het} and J_{het} increase exponentially with decreasing T. In some instances, values of ω_{het} and J_{het} for different a_w overlap each other. This behavior may be due to a temperature dependence of or uncertainty in a_w. According to classical nucleation theory, ω_{het} and J_{het} reflects an exponential dependence on temperature (Pruppacher and Klett, 1997) suggesting that heterogeneous ice nucleation due to intact and fragmented diatoms follows a time-dependent freezing process, in line with classical nucleation theory.

3.2.2 Time-independent analysis

A time-independent approach (Vali, 1971) can also be used to quantify heterogeneous ice nucleation due to intact and fragmented diatoms. This mechanistic explanation commonly referred to as the singular approach, maintains that the freezing process is dominated by an active site on the surface of a particle which triggers ice nucleation at a specific characteristic temperature.

Following a previously described analysis by Vali (1971), we derive differential and cumulative nuclei spectra to quantify a time-independent approach for explaining heterogeneous ice nucleation due to diatoms. The differential nuclei spectra for the i-th temperature interval, $k(T^i)$, is defined as

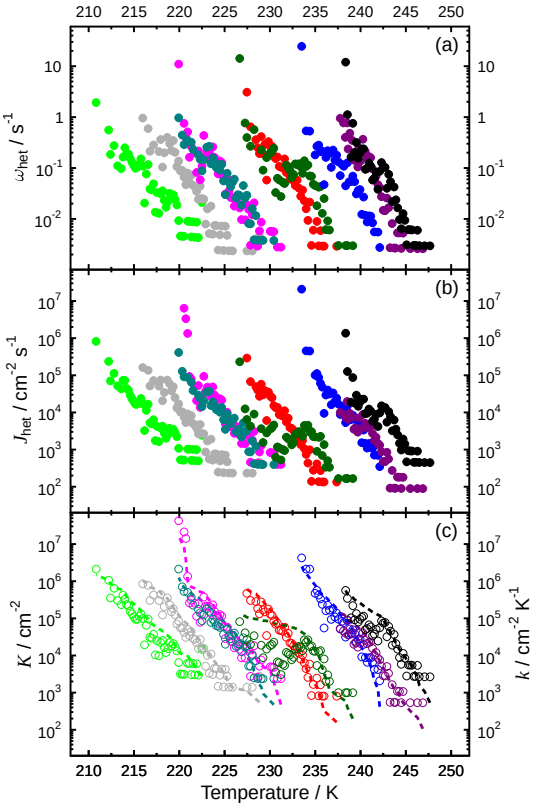

Fig. 8. Experimentally derived **(a)** heterogeneous ice nucleation rates, ω_{het}, **(b)** heterogeneous ice nucleation rate coefficients, J_{het}, and **(c)** differential and cumulative nuclei spectra, $k(T)$ and $K(T)$, respectively, for aqueous NaCl/diatom droplets shown as a function of T and a_w. In **(c)**, the $k(T)$ and $K(T)$ are given as open circles and dotted lines, respectively. Black, purple, blue, green, red, teal, magenta, gray, and lime colors correspond to aqueous NaCl droplets containing diatoms with initial a_w of 0.984, 0.969, 0.951, 0.926, 0.902, 0.873, 0.850, 0.826, 0.800.

the ice active surface site density for a unit surface area of a sample

$$k(T^i) = \frac{1}{A^i_{tot}} \frac{n^i_{nuc}}{\Delta T}, \quad (9)$$

where A^i_{tot} is the total diatom surface area in the droplets that remains liquid at the start of the i-th temperature interval (Vali, 1971). A cumulative nucleus spectrum as a function of temperature, $K(T^i)$, can be evaluated from experimental data by numerically integrating Eq. (9) from T^{dia}_m to T^i yielding

$$K(T^i) = \sum_{T^{dia}_m}^{T_i} \frac{n^i_{nuc}}{A^i_{tot}}, \quad (10)$$

where $K(T^i)$ includes the sites which had become ice active for temperatures warmer than T^i. Derivations of $k(T)$ and $K(T)$ employ $\Delta T = 0.2$ K.

Figure 8c presents $k(T)$ and $K(T)$ for the individually analyzed ice nucleation events presented in Fig. 7 as a function of T and a_w. Figure 8c demonstrates that $k(T)$ for most data increases exponentially with decreasing T. As previously described, $k(T)$ is the differential spectrum for $K(T)$ and thus it follows from Eqs. (9) and (10) that $k(T) = dK(T)/dT$. Since $k(T)$ shows an exponential behavior, $K(T)$ also increases exponentially with deceasing temperature for ice nucleation events at specific a_w. In some instances, values of $k(T)$ and $K(T)$ for different a_w overlap each other. Similar to the time-dependent approach, this behavior may be due to a temperature dependence of or uncertainty in a_w.

3.2.3 Water activity and heterogeneous ice nucleation

Figure 4 indicates that the water activity criterion can also be used to predict median freezing temperatures of heterogeneous ice nucleation (Koop and Zobrist, 2009). Table 1 gives ω_{het}, J_{het}, and $K(T)$ evaluated at the median freezing temperatures shown in Fig. 4. On average and over the range of investigated a_w values, $\omega_{het}(T^{dia}_f) = 0.11^{+0.06}_{-0.05}$ s^{-1}, $J_{het}(T^{dia}_f) = 1.0^{+1.16}_{-0.61} \times 10^4$ cm^{-2} s^{-1}, and $K(T^{dia}_f) = 6.2^{+3.5}_{-4.1} \times 10^4$ cm^{-2} for aqueous NaCl/diatom droplets, where the plus and minus errors indicate the range in values. The narrow range of ω_{het}, J_{het}, and $K(T)$ along the freezing line indicates that the shifted a^{ice}_w curve shown in Fig. 4 is representative of these freezing rates and nuclei spectra. This further supports the contention that immersion mode freezing can be parameterized by $\Delta a_{w,het}$. Here, we report that a shift of $\Delta a_{w,het} = 0.2303$ describes heterogeneous ice nucleation temperatures for immersion freezing where $\omega_{het}(T^{dia}_f) = 0.11$ s^{-1}, $J_{het}(T^{dia}_f) = 1.0 \times 10^4$ cm^{-2} s^{-1}, and $K(T^{dia}_f) = 6.2 \times 10^4$ cm^{-2}. Further studies are necessary to investigate whether ω_{het}, J_{het}, and $K(T)$ can be similarly parameterized as a function of a_w as for the case of homogeneous ice nucleation (Koop et al., 2000b).

4 Atmospheric implications

4.1 Homogeneous ice nucleation

The results of the homogeneous freezing experiments reported here allow for a better constraint of predicted J_{hom} from aqueous NaCl droplets and can be used to narrow the uncertainty in the theoretical predictions of the water activity based homogeneous ice nucleation theory (Koop et al., 2000b; Koop, 2004; Koop and Zobrist, 2009; Knopf and Rigg, 2011). This is significant because an uncertainty of 0.025 in a_w can lead to changes in J_{hom} of up to 6 orders of magnitude or 8 K in temperature (Koop, 2004; Knopf and Lopez, 2009; Knopf and Rigg, 2011). In addition, the derivation of J_{hom} allows for estimation of ice particle production rates from derived homogeneous nucleation according to $P^{ice}_{hom} = J_{hom} \cdot V_{particle}$, where $V_{particle}$ is the amount of total

liquid volume of aerosol per cm^3 of air. We assume sea salt concentrations, estimated here from field observations of aerosol particle concentrations in the free troposphere as $10\,cm^{-3}$ (Cziczo et al., 2004; Ikegami et al., 1994, 2004; Brock et al., 2011; Hara et al., 2006), with mean dry diameter of 200 nm and a wet diameter of 480 nm at 90 % RH (Zhang et al., 2005; Lewis and Schwartz, 2006), and applying $J_{hom} = 10^6\,cm^{-3}\,s^{-1}$ at a temperature of 215 K (Fig. 3), P_{hom}^{ice} could reach 0.035 ice particles L^{-1} (air) min^{-1}. Ice crystal concentrations in cirrus clouds usually fall between 10 and $100\,L^{-1}$ (air) (Dowling and Radke, 1990; Heymsfield and McFarquhar, 2002; Haag et al., 2003; Strom et al., 2003). Thus, after 30 min at these atmospheric conditions, approximately 1 ice crystal per liter of air could form.

4.2 Heterogeneous ice nucleation

As far as we are aware, neither spatial and temporal concentrations nor corresponding determination of surface areas of aerosolized diatoms are available. In fact, we are only aware of two studies which have reported airborne diatom concentrations. A study by Tormo et al. (2001) observed airborne diatoms in excess of $0.07\,L^{-1}$ (air) in summer outside the city of Badajoz, SW Spain, about 100 m away from the Gevora River. We would expect that airborne concentrations of diatoms would be greater over marine waters where wave action can result in greater generation of sea spray and bubble bursting aerosols when compared with rivers. In fact, a study in which filter samples were collected from a 9 m high tower on a 55 m high cliff off the coast on Amsterdam Island (a tiny remote volcanic island in the Southern Indian Ocean some 3000 km from any continent) found concentrations of marine biogenic particles characterized as amorphous silica diatom fragments, ranging from $\sim$20–28 L^{-1} of air (Gaudichet et al., 1989). While not specifically reporting size distributions, ambient insoluble particles from their air samples had mean diameters of $\simeq (0.8 \pm 0.7)$ µm (Gaudichet et al., 1989). Brown et al. (1964) found a diversity of viable airborne algal species in concentrations as high as $4\,L^{-1}$ (air), suggesting that this number would be greater if nonviable algae were additionally counted. Concentrations of marine bacteria in air originating from ocean waters is estimated to be on the order of $10\,L^{-1}$ (air) (Burrows et al., 2009b), which can provide an upper limit on airborne diatom concentrations assuming similar processes that lead to aerosolization of diatoms. If, however, diatom fragments are aerosolized or whole diatoms are fragmented in the atmosphere, i.e. during dust transport (Harper, 1999), then concentrations can actually exceed those of bacteria, given that one whole diatom would be broken into smaller and more numerous fragments. IN concentration at $-15\,°C$ taken in air over the Arctic Ocean show a positive correlation with particle sizes between 50 nm and 120 nm (Bigg, 2001), smaller than sizes of viable airborne bacteria that are typically $\sim$4 µm (Shaffer and Lighthart, 1997; Burrows et al., 2009a). Diatom fragments would be expected to fall within this size range which could explain the correlation with IN concentrations measured by Bigg (2001). Lastly, a very recent study found a unique organic marine aerosol mass concentration of up to $3.8\,µg\,m^{-3}$ in an aerosol plume passing over highly productive surface waters in the North Atlantic off Mace Head (Ovadnevaite et al., 2011).

From the above discussion, we estimate a conservative lower limit of airborne diatom fragment concentrations of $0.1\,L^{-1}$ (air). In cases of high biological production and strong wave activity, this number may be 2 orders of magnitude higher. The major contribution of primary organic matter to sea spray aerosol have been found to be in the submicrometer size range (O'Dowd et al., 2004; Ovadnevaite et al., 2011) and thus, we assume a maximum size of a diatom fragment to be 1 µm. This provides an upper estimate for the corresponding surface dependent ice particle production. We expect that these estimates will vary with additional field collected data.

In the case that ice nucleation induced by intact or fragmented diatoms is assumed to be independent of surface area, we can derive ice particle production rates as a function of T and RH, $P_{het}^{ice}(T, RH)$, as

$$P_{het}^{ice}(T, RH) = \omega_{het}(T, RH) \cdot N_{particle}, \quad (11)$$

where $N_{particle}$ is the total diatom concentration per unit volume of air and ω_{het} is determined from Fig. 8a for given T and RH.

If available diatom surface area is accounted for in the description of heterogeneous ice nucleation then,

$$P_{het}^{ice}(T, RH) = J_{het}(T, RH) \cdot S_{particle}, \quad (12)$$

and

$$P_{het}^{ice}(T) = K(T, RH) \cdot S_{particle}. \quad (13)$$

$J_{het}(T, RH)$ and $K(T, RH)$ are determined from Fig. 8b, c. $S_{particle}$ is the total diatom surface area per unit volume of air. Following the arguments presented above, we assume that the diatom fragments are a square plate with side length of 1 µm resulting in a surface area of 2 $µm^2$ per diatom particle and therefore, $2 \times 10^{-9}\,cm^2\,L^{-1}$ of air given diatom concentrations of $0.1\,L^{-1}$ (air). Equations (11) and (12) describe time-dependent ice particle production whereas Eq. (13) yields ice particle production as a function of temperature reflecting the fundamental differences in the description of the ice nucleation process.

We now estimate ice particle production for the two following scenarios: (i) Ice formation at conditions typical for Arctic mixed-phase clouds. (ii) Ice formation at typical cirrus cloud temperatures of about 220 K.

Assuming diatom concentrations of $0.1\,L^{-1}$ (air) and RH = 95 %, we derive for $T = 240\,K$ and corresponding $\omega_{het} = 0.11\,s^{-1}$, $P_{het}^{ice} = 0.7$ ice particles L^{-1} (air) min^{-1}. This indicates that all available diatoms would nucleate ice

within seconds. Assuming the ice nucleation process to be surface dependent and applying $J_{het} = 1.0 \times 10^4\,cm^{-2}\,s^{-1}$ and $K = 6.2 \times 10^4 cm^{-2}$, the corresponding P_{het}^{ice} is equal to $0.001\,L^{-1}$ (air) min^{-1} and $0.0001\,L^{-1}$ (air), respectively. From this example, it follows that the time-dependent analysis will always yield higher ice particle numbers with time at fixed temperatures (or small updraft velocities) compared to analysis using the time-independent approach. Typical ice crystal concentrations observed in Arctic mixed-phase clouds are $\sim$0.1–10 L^{-1} (air) (McFarquhar et al., 2007; Fridlind et al., 2007; Verlinde et al., 2007). Thus, if a minor fraction of background sea salt particles contains diatoms or fragments of diatoms, then a significant amount of ice crystal production could be attributable to diatoms if ice nucleation follows a time-dependent mechanism. IN concentrations in polar regions can be greater in summer than those in winter and fall months (Bigg, 1996; Rogers et al., 2001b; McFarquhar et al., 2007; Prenni et al., 2009), and can coincide with phytoplankton blooms in the surface waters below (Bigg, 1973; Schnell, 1975; Schnell and Vali, 1976). This seasonality may be attributable to aerosolized diatoms acting as IN.

At $T = 220\,K$ and RH = 85 % (Haag et al., 2003; Strom et al., 2003) applying the same diatom concentration for cirrus cloud formation assuming ice nucleation does not depend on surface area, we derive $\omega_{het} = 0.51\,s^{-1}$ and $P_{het}^{ice} = 3.06$ ice particles L^{-1} (air) min^{-1}. This indicates that all available diatoms would nucleate ice within seconds. Accounting for the surface dependence of the ice nucleation process, we can employ $J_{het} = 1.8 \times 10^5\,cm^{-2}\,s^{-1}$ and $K = 1.1 \times 10^6\,cm^{-2}$ which yield corresponding $P_{het}^{ice} = 0.022\,L^{-1}$ (air) min^{-1} and $P_{het}^{ice} = 0.0022\,L^{-1}$ (air), respectively. As in the previous example, for a fixed or slowly decreasing temperature, the time-dependent nucleation description will always result in higher ice crystal concentrations. Thus, predictions of ice crystal production are sensitive to the choice of either a time-dependent or time-independent approach.

Typical ice crystal concentrations observed in cirrus clouds due to heterogeneous ice nucleation can be expected to be greatly affected by depletion of water vapour subsequent to ice crystal formation according to the Bergeron-Wegener-Findeisen process (Bergeron, 1935; Wegener, 1911; Findeisen, 1938), rapid ice particle production through riming according to the Hallett-Mossop effect (Hallett and Mossop, 1974; Mossop and Hallett, 1974), and the presence of other IN. Thus, ice crystal concentrations in cirrus clouds impacted by heterogeneous ice nucleation are ill defined and remain largely uncertain (Cantrell and Heymsfield, 2005). As previously mentioned, cirrus clouds typically have ice crystal concentrations of 10–100 L^{-1} (air). Our calculations indicate that a time-dependent approach will result in rapid ice crystal production rates so that after approximately 5 to 10 min at a constant or slowly changing temperature, diatoms could significantly impact cirrus cloud formation. On the other hand, this does not apply when employing a time-independent approach for ice particle production resulting in ice crystal numbers lower than typical observations.

From these estimates, it remains unclear whether it is more appropriate to apply either a time-dependent or time-independent approach for determination of ice crystal production or if a combination of the two would be more appropriate (Pruppacher and Klett, 1997; Marcolli et al., 2007; Vali, 2008). For a given temperature, the difference between the two theoretical approaches is about 2 orders of magnitude. While this seems small compared to typical uncertainties in ice nucleation rate predictions, the cloud microphysical evolution would proceed in significantly different directions depending on which nucleation mechanism is assumed to be taking place. Of course this discussion serves only as an example and is simplified compared to the actual progression within the cloud formation process. We therefore recommend taking advantage of cloud system resolving models with a high time resolution (Kärcher and Lohmann, 2003; Phillips et al., 2009) to evaluate the sensitivity of time-dependent and time-independent ice crystal production utilizing the results presented here for heterogeneous ice nucleation due to marine biogenic particles as represented by diatoms.

5 Summary

Homogeneous and heterogeneous freezing of ice from micrometer-sized aqueous NaCl droplets with and without diatoms have been analyzed in the temperature range of 180 to 260 K and for water activities of 0.8 to 0.99. The freezing of about 5000 individual droplets has been investigated in this study.

The median homogeneous freezing temperatures agreed, within experimental and theoretical uncertainties, with predictions of the water-activity based homogeneous ice nucleation theory. The experimentally derived homogeneous ice nucleation rate coefficients were in agreement with predictions of the water-activity based theory and can be employed to further constrain that theory. Corresponding ice particle production rates were derived from experimentally obtained homogeneous ice nucleation rate coefficients.

The median heterogeneous freezing temperatures due to intact and fragmented diatoms were well represented by the modified water-activity based theory, where a horizontal shift by $\Delta a_{w,het} = 0.2303$ of the corresponding ice melting curve describes the experimentally derived freezing data. Diatom surface area and aqueous volume were determined for every droplet investigated. Under our experimental conditions, heterogeneous freezing temperatures neither depended on the droplet volume nor on the available diatom surface area. The heterogeneous ice nucleation rate evaluated at median freezing temperatures, represented by the shifted melting curve,

is $0.11^{+0.06}_{-0.05}\,s^{-1}$. Assuming that ice nucleation depends on surface area we derive heterogeneous ice nucleation rate coefficients and time-independent cumulative nuclei spectra as $1.0^{+1.16}_{-0.61}\times10^4\,cm^{-2}\,s^{-1}$ and $6.2^{+3.5}_{-4.1}\times10^4\,cm^{-2}$, respectively. Assuming diatom concentrations of $0.1\,L^{-1}$, corresponding ice particle production rates indicate that intact and fragments of diatoms can efficiently form ice crystals under typical tropospheric conditions. Ice particle production assuming a time-dependent nucleation mechanism is always greater at slow updrafts or slowly changing temperatures when compared with a time-independent nucleation process. High resolution cloud system resolving models can be used to evaluate the sensitivity of ice particle production in response to intact and fragmented diatoms by either time-dependent or time-independent analyses.

Acknowledgements. We thank N. Fisher and S. Palma for providing diatom cultures, J. Radway for assistance in diatom preparation, and J. Quinn for recording SEM images. This work was supported by the NOAA Climate Program Office, Atmospheric Composition and Climate Program, Grant NA08OAR4310545.

Edited by: O. Möhler

References

Albrecht, B. A.: Aerosols, cloud microphysics, and fractional cloudiness, Science, 245, 1227–1230, 1989.

Aller, J. Y., Kuznetsova, M. R., Jahns, C. J., and Kemp, P.: The sea surface microlayer as a source of viral and bacterial enrichment in marine aerosols, J. Aerosol. Sci., 36, 801–812, 2005.

Alvain, S., Moulin, C., Dandonneau, Y., and Loisel, H.: Seasonal distribution and succession of dominant phytoplankton groups in the global ocean: a satellite view, Global Biogeochem. Cy., 22, GB3001, doi:10.1029/2007GB003154, 2008.

Anderson, T. L., Charlson, R. J., Schwartz, S. E., Knutti, R., Boucher, O., Rodhe, H., and Heintzenberg, J.: Climate forcing by aerosols – a hazy picture, Science, 300, 1103–1104, 2003.

Andreae, M. O. and Crutzen, P. J.: Atmospheric aerosols: biogeochemical sources and role in atmospheric chemistry, Science, 276, 1052–1058, 1997.

Baker, M. B.: Cloud microphysics and climate, Science, 276, 1072–1078, 1997.

Baker, M. B. and Peter, T.: Small-scale cloud processes and climate, Nature, 451, 299–300, 2008.

Bergeron, T.: On the physics of clouds and precipitation, Proc. 5th Assembly U.G.G.I., Lisbon, 14–23 September, 2, p. 156, 1935.

Bertram, A. K., Koop, T., Molina, L. T., and J., M. M.: Ice formation in $(NH_4)_2SO_4$-H_2O particles, J. Phys. Chem. A, 104, 584–588, 2000.

Bigg, E. K.: The supercooling of water, P. Phys. Soc. B, 66, 688–694, 1953.

Bigg, E. K.: Ice nucleus concentrations in remote areas, J. Atmos. Sci., 30, 1153–1157, 1973.

Bigg, E. K.: Ice forming nuclei in the high Arctic, Tellus B, 48, 223–233, 1996.

Bigg, E. K. and Leck, C.: Cloud-active particles over the central Arctic Ocean, J. Geophys. Res., 106(D23), 32155–32166, doi:10.1029/1999JD901152, 2001.

Bigg, E. K. and Leck, C.: The composition of fragments of bubbles bursting at the ocean surface, J. Geophys. Res., 113, D11209, doi:10.1029/2007jd009078, 2008.

Blanchard, D. C.: Bubble scavenging and water-to-air-transfer of organic material in the sea, Adv. Chem. Ser., 145, 360–387, 1975.

Blanchard, D. C. and Syzdek, L.: Mechanism for water-to-air transfer and concentration of bacteria, Science, 170, 626–628, 1970.

Borys, R. D.: The effects of long range transport of air pollutants on Arctic cloud active aerosol, Ph.D. thesis, Dept. Atmos. Sci. Colorado State Univ., Ft. Collins, USA, 1983.

Brock, C. A., Cozic, J., Bahreini, R., Froyd, K. D., Middlebrook, A. M., McComiskey, A., Brioude, J., Cooper, O. R., Stohl, A., Aikin, K. C., de Gouw, J. A., Fahey, D. W., Ferrare, R. A., Gao, R.-S., Gore, W., Holloway, J. S., Hübler, G., Jefferson, A., Lack, D. A., Lance, S., Moore, R. H., Murphy, D. M., Nenes, A., Novelli, P. C., Nowak, J. B., Ogren, J. A., Peischl, J., Pierce, R. B., Pilewskie, P., Quinn, P. K., Ryerson, T. B., Schmidt, K. S., Schwarz, J. P., Sodemann, H., Spackman, J. R., Stark, H., Thomson, D. S., Thornberry, T., Veres, P., Watts, L. A., Warneke, C., and Wollny, A. G.: Characteristics, sources, and transport of aerosols measured in spring 2008 during the aerosol, radiation, and cloud processes affecting Arctic Climate (ARCPAC) Project, Atmos. Chem. Phys., 11, 2423–2453, doi:10.5194/acp-11-2423-2011, 2011.

Brown, R. M., Larson, D. A., and Bold, H. C.: Airborne algae: their abundance and heterogeneity, Science, 143, 583–585, 1964.

Burrows, S. M., Butler, T., Jöckel, P., Tost, H., Kerkweg, A., Pöschl, U., and Lawrence, M. G.: Bacteria in the global atmosphere – Part 2: Modeling of emissions and transport between different ecosystems, Atmos. Chem. Phys., 9, 9281–9297, doi:10.5194/acp-9-9281-2009, 2009a.

Burrows, S. M., Elbert, W., Lawrence, M. G., and Pöschl, U.: Bacteria in the global atmosphere – Part 1: Review and synthesis of literature data for different ecosystems, Atmos. Chem. Phys., 9, 9263–9280, doi:10.5194/acp-9-9263-2009, 2009b.

Cantrell, W. and Heymsfield, A.: Production of ice in tropospheric clouds: a review, B. Am. Meteorol. Soc., 86, 795–807, 2005.

Chalmers, M. O., Harper, M. A., and Marshall, W. A.: An Illustrated Catalogue of Airborne Microbiota from the Maritime Antarctic, British Antarctic Survey, National Environmental Research Council, High Cross, Madingley Road, Cambridge, CB3 0ET, UK, 1–175, 1996.

Charlson, R. J., Schwartz, S. E., Hales, J. M., Cess, R. D., Coakley, J. A., Hansen, J. E., and Hofmann, D. J.: Climate forcing by anthropogenic aerosols, Science, 255, 423–430, 1992.

Clarke, E. C. W. and Glew, D. N.: Evaluation of the thermodynamic functions for aqueous sodium-chloride from equilibrium and calorimetric measurements below 154 °C, J. Phys. Chem. Ref. Data, 14, 489–610, 1985.

Clegg, S. L., Brimblecombe, P., and Wexler, A. S.: A thermodynamic model of the system H^+–NH_4^+–Na^+–SO_4^{2-}–NO_3^-–Cl^-–H_2O at 298.15 K, J. Phys. Chem. A, 102, 2155–2171, available online at: http://www.aim.env.uea.ac.uk/aim/aim.php (last access: May 2010), 1998.

Cziczo, D. J., Murphy, D. M., Hudson, P. K., and Thomson, D. S.:

Single particle measurements of the chemical composition of cirrus ice residue during CRYSTAL-FACE, J. Geophys. Res., 109, D04201, doi:10.1029/2003JD004032, 2004.

Dall'Osto, M., Ceburnis, D., Martucci, G., Bialek, J., Dupuy, R., Jennings, S. G., Berresheim, H., Wenger, J., Healy, R., Facchini, M. C., Rinaldi, M., Giulianelli, L., Finessi, E., Worsnop, D., Ehn, M., Mikkilä, J., Kulmala, M., and O'Dowd, C. D.: Aerosol properties associated with air masses arriving into the North East Atlantic during the 2008 Mace Head EUCAARI intensive observing period: an overview, Atmos. Chem. Phys., 10, 8413–8435, doi:10.5194/acp-10-8413-2010, 2010.

Darwin, C.: An account of the fine dust which often falls on vessels in the Atlantic Ocean, Q. J. Geo. Soc., 2, 26–30, 1846.

De Haan, D. O., Brauers, T., Oum, K., Stutz, J., Nordmeyer, T., and Finlayson-Pitts, B. J.: Heterogeneous chemistry in the troposphere: experimental approaches and applications to the chemistry of sea salt particles, Int. Rev. Phys. Chem., 18, 343–385, 1999.

DeMott, P. J., Rogers, D. C., Kreidenweis, S. M., Chen, Y., Twohy, C. H., Baumgardner, D., Heymsfield, A. J., and Chan, K. R.: The role of heterogeneous freezing in upper tropospheric clouds: inferences from SUCCESS, Geophys. Res. Lett., 25, 1387–1390, 1998.

DeMott, P. J., Sassen, K., Poellot, M. R., Baumgardner, D., Rogers, D. C., Brooks, S. D., Prenni, A. J., and Kreidenweis, S. M.: African dust aerosols as atmospheric ice nuclei, Geophys. Res. Lett., 30(14), 1732, doi:10.1029/2003GL017410, 2003.

Dorsey, N. E.: The freezing of supercooled water, T. Am. Philos. Soc., 38, 247–328, 1948.

Dowling, D. R. and Radke, L. F.: A summary of the physical properties of cirrus clouds, J. Appl. Meteorol., 29, 970–978, 1990.

Fall, R. and Schnell, R. C.: Association of an ice-nucleating *Pseudomonad* with cultures of the marine *Dinoflagellate*, *heterocapsa-niei*, J. Mar. Res., 43, 257–265, 1985.

Findeisen, W.: Die kolloidmeteorologischen Vorgänge bei der Niederschlagsbildung (Colloidal meteorological processes in the formation of precipitation), Meteorol. Z., 55, 121–133, 1938.

Finlayson-Pitts, B. J.: The tropospheric chemistry of sea salt: a molecular-level view of the chemistry of NaCl and NaBr, Chem. Rev., 103, 4801–4822, 2003.

Fisher, N. S. and Wente, M.: The release of trace-elements by dying marine-phytoplankton, Deep-Sea Res. Pt. I, 40, 671–694, 1993.

Flyger, H. and Heidam, N. Z.: Ground level measurements of summer tropospheric aerosol in Northern Greenland, J. Aerosol Sci., 9, 157–168, 1978.

Forster, P., Ramaswamy, V., Artaxo, P., Berntsen, T., Betts, R., Fahey, D. W., Haywood, J., Lean, J., Lowe, D. C., Myhre, G., Nganga, J., Prinn, R., Raga, G., Schulz, M., and Van Dorland, R.: Changes in Atmospheric Constituents and in Radiative Forcing, in: Climate Change 2007: The Physical Science Basis. Contribution of Working Group I to the Fourth Assessment Report of the Intergovernmental Panel on Climate Change, chap. 2, edited by: Solomon, S., Qin, D., Manning, M., Chen, Z., Marquis, M., Averyt, K. B., Tignor, M., and Miller, H. L. Cambridge University Press, Cambridge, UK and New York, NY, USA, 131–234, 2007.

Fridlind, A. M., Ackerman, A. S., McFarquhar, G., Zhang, G., Poellot, M. R., DeMott, P. J., Prenni, A. J., and Heymsfield, A. J.: Ice properties of single-layer stratocumulus during the Mixed-Phase Arctic Cloud Experiment: 2. Model results, J. Geophys. Res., 112, D24202, doi:10.1029/2007jd008646, 2007.

Gaudichet, A., Lefévre, R., Gaudry, A., Ardouin, B., Lambert, G., and Miller, J. M.: Mineralogical composition of aerosols at Amsterdam Island, Tellus, 41B, 344–352, 1989.

Ghan, S. J., Guzman, G., and Abdul-Razzak, H.: Competition between sea salt and sulfate particles as cloud condensation nuclei, J. Atmos. Sci., 55, 3340–3347, 1998.

Guillard, R. R. and Ryther, J. H.: Studies of marine planktonic diatoms: I. *Cyclotella nana* Hustedt, and *Detonula confervacea* (Cleve) Gran, Can. J. Microbiol., 8, 229–239, 1962.

Haag, W., Kärcher, B., Ström, J., Minikin, A., Lohmann, U., Ovarlez, J., and Stohl, A.: Freezing thresholds and cirrus cloud formation mechanisms inferred from in situ measurements of relative humidity, Atmos. Chem. Phys., 3, 1791–1806, doi:10.5194/acp-3-1791-2003, 2003.

Hakansson, H. and Nihlen, T.: Diatoms of eolian deposits in the Mediterranean, Arch. Protistenk., 138, 313–322, 1990.

Hallett, J. and Mossop, S. C.: Production of secondary ice particles during riming process, Nature, 249, 26–28, 1974.

Hara, K., Iwasaka, Y., Wada, M., Ihara, T., Shiba, H., Osada, K., and Yamanouchi, T.: Aerosol constituents and their spatial distribution in the free troposphere of coastal Antarctic regions, J. Geophys. Res., 111, D15216, doi:10.1029/2005JD006591, 2006.

Harper, M. A.: Diatoms as markers of atmospheric transport, in: The Diatoms: Applications for the Environmental and Earth Sciences, chap. 22, edited by: Stoermer, E. F. and Smol, J. P., Cambridge University Press, Cambridge, 429–435, 1999.

Hegg, D. A. and Baker, M. B.: Nucleation in the atmosphere, Rep. Prog. Phys., 72, 056801, doi:10.1088/0034-4885/72/5/056801, 2009.

Heymsfield, A. J. and McFarquhar, G. M.: Mid-Latitude and Tropical Cirrus: Microphysical Properties, Oxford University Press, 198 Madison Avenue, New York, New York 10016, USA, 2002.

Heymsfield, A. J., Miloshevich, L. M., Twohy, C., Sachse, G., and Oltmans, S.: Upper tropospheric relative humidity observations and implications for cirrus ice nucleation, Geophys. Res. Lett., 25, 1343–1350, 1998.

Hobbie, J. E., Daley, R. J., and Jasper, S.: Use of nuclepore filters for counting bacteria by fluorescence microscopy, Appl. Enivron. Microb., 33, 1225–1228, 1977.

Ikegami, M., Okada, K., Zaizen, Y., and Makino, Y.: Sea-salt particles in the upper tropical troposphere, Tellus Ser. B-Chem. Phys. Meteorol., 46, 142–151, 1994.

Ikegami, M., Okada, K., Zaizen, Y., Tsutsumi, Y., Makino, Y., Jensen, J. B., and Gras, J. L.: The composition of aerosol particles in the middle troposphere over the western Pacific Ocean: aircraft observations from Australia to Japan, January 1994, Atmos. Environ., 38, 5945–5956, 2004.

Junge, K. and Swanson, B. D.: High-resolution ice nucleation spectra of sea-ice bacteria: implications for cloud formation and life in frozen environments, Biogeosciences, 5, 865–873, doi:10.5194/bg-5-865-2008, 2008.

Kärcher, B. and Lohmann, U.: A parameterization of cirrus cloud formation: heterogeneous freezing, J. Geophys. Res., 108, 4402, doi:10.1029/2002JD003220, 2003.

Kaufman, Y. J., Tanrá, D., and Boucher, O.: A satellite view of

aerosols in the climate system, Nature, 419, 215–223, 2002.
Kawai, S.: Preliminary observations of the diatoms in atmosphere, Int. Aerobio. Newsl., 15, 6–10, 1981.
Kellogg, D. E. and Kellogg, T. B.: Diatoms in South Pole ice: implications for eolian contamination of sirius group deposits, Geology, 24, 115–118, 1996.
Knopf, D. A.: Do NAD and NAT form in liquid stratospheric aerosols by pseudoheterogeneous nucleation?, J. Phys. Chem. A, 110, 5745–5750, 2006.
Knopf, D. A. and Lopez, M. D.: Homogeneous ice freezing temperatures and ice nucleation rates of aqueous ammonium sulfate and aqueous levoglucosan particles for relevant atmospheric conditions, Phys. Chem. Chem. Phys., 11, 8056–8068, 2009.
Knopf, D. A. and Rigg, Y. J.: Homogeneous ice nucleation from aqueous inorganic/organic particles representative of biomass burning: water activity, freezing temperatures, nucleation rates, J. Phys. Chem. A, 115, 762–773, doi:10.1021/jp109171g, 2011.
Knopf, D. A., Koop, T., Luo, B. P., Weers, U. G., and Peter, T.: Homogeneous nucleation of NAD and NAT in liquid stratospheric aerosols: insufficient to explain denitrification, Atmos. Chem. Phys., 2, 207–214, doi:10.5194/acp-2-207-2002, 2002.
Knopf, D. A., Luo, B. P., Krieger, U. K., and Koop, T.: Thermodynamic dissociation constant of the bisulfate ion from raman and ion interaction modeling studies of aqueous sulfuric acid at low temperatures, J. Phys. Chem. A, 107, 4322–4332, 2003.
Knopf, D. A., Wang, B., Laskin, A., Moffet, R. C., and Gilles, M. K.: Heterogeneous nucleation of ice on anthropogenic organic particles collected in Mexico City, J. Geophys. Res., 37, L11803, doi:10.1029/2010GL043362, 2010.
Knopf, D. A., Alpert, P. A., Wang, B., and Aller, J. Y.: Stimulation of ice nucleation by marine diatoms, Nat. Geosci., 4, 88–90, doi:10.1038/ngeo1037, 2011.
Koop, T.: Homogeneous ice nucleation in water and aqueous solutions, Z. Phys. Chem., 218, 1231–1258, 2004.
Koop, T. and Zobrist, B.: Parameterizations for ice nucleation in biological and atmospheric systems, Phys. Chem. Chem. Phys., 11, 10839–10850, 2009.
Koop, T., Luo, B. P., Biermann, U. M., Crutzen, P. J., and Peter, T.: Freezing of $HNO_3/H_2SO_4/H_2O$ solutions at stratospheric temperatures: nucleation statistics and experiments, J. Phys. Chem. A, 101, 1117–1133, 1997.
Koop, T., Ng, H. P., Molina, L. T., and Molina, M. J.: A new optical technique to study aerosol phase transitions: the nucleation of ice from H_2SO_4 aerosols, J. Phys. Chem. A, 102, 8924–8931, 1998.
Koop, T., Kapilashrami, A., Molina, L. T., and Molina, M. J.: Phase transitions of sea-salt/water mixtures at low temperatures: implications for ozone chemistry in the polar marine boundary layer, J. Geophys. Res., 105, 26393–26402, 2000a.
Koop, T., Luo, B. P., Tsias, A., and Peter, T.: Water activity as the determinant for homogeneous ice nucleation in aqueous solutions, Nature, 406, 611–614, 2000b.
Kuznetsova, M., Lee, C., and Aller, J.: Characterization of the proteinaceous matter in marine aerosols, Mar. Chem., 96, 359–377, 2005.
Lewis, E. R. and Schwartz, S. E.: Comment on "size distribution of sea-salt emissions as a function of relative humidity", Atmos. Environ., 40, 588–590, 2006.
Linke, W. F.: Solubilities of Inorganic and Metal Organic Compounds, Am. Chem. Soc., Washington DC, USA, 958–959, 1965.
Lohmann, U. and Feichter, J.: Global indirect aerosol effects: a review, Atmos. Chem. Phys., 5, 715–737, doi:10.5194/acp-5-715-2005, 2005.
Marcolli, C., Gedamke, S., Peter, T., and Zobrist, B.: Efficiency of immersion mode ice nucleation on surrogates of mineral dust, Atmos. Chem. Phys., 7, 5081–5091, doi:10.5194/acp-7-5081-2007, 2007.
McComiskey, A., Schwartz, S. E., Schmid, B., Guan, H., Lewis, E. R., Ricchiazzi, P., and Ogren, J. A.: Direct aerosol forcing: calculation from observables and sensitivities to inputs, J. Geophys. Res., 113, D09202, doi:10.1029/2007JD009170, 2008.
McFarquhar, G. M., Zhang, G., Poellot, M. R., Kok, G. L., McCoy, R., Tooman, T., Fridlind, A., and Heymsfield, A. J.: Ice properties of single-layer stratocumulus during the Mixed-Phase Arctic Cloud Experiment: 1. Observations, J. Geophys. Res., 112, D24201, doi:10.1029/2007jd008633, 2007.
McKay, R. M., Barrett, P. J., Harper, M. A., and Hannah, M. J.: Atmospheric transport and concentration of diatoms in surficial and glacial sediments of the Allan Hills, Transantarctic Mountains, Palaeogeo. Palaeocli. Palaeoecol., 260, 168–183, 2008.
Mossop, S. C. and Hallett, J.: Ice crystal concentration in cumulus clouds: influence of the drop spectrum, Science, 186, 632–633, 1974.
Murphy, D. M. and Koop, T.: Review of the vapour pressures of ice and supercooled water for atmospheric applications, Q. J. Roy. Meteorol. Soc., 131, 1539–1565, 2005.
O'Dowd, C. D., Smith, M. H., Consterdine, I. E., and Lowe, J. A.: Marine aerosol, sea-salt, and the marine sulphur cycle: a short review, Atmos. Environ., 31, 73–80, 1997.
O'Dowd, C. D., Lowe, J. A., and Smith, M. H.: Coupling sea-salt and sulphate interactions and its impact on cloud droplet concentration predictions, Geophys. Res. Lett., 26, 1311–1314, 1999.
O'Dowd, C. D., Facchini, M. C., Cavalli, F., Ceburnis, D., Mircea, M., Decesari, S., Fuzzi, S., Yoon, Y. J., and Putaud, J. P.: Biogenically driven organic contribution to marine aerosol, Nature, 431, 676–680, 2004.
Ovadnevaite, J., O'dowd, C., Dall'Osto, M., Ceburnis, D., Worsnop, D. R., and Berresheim, H.: Detecting high contributions of primary organic matter to marine aerosol: a case study, J. Geophys. Res., 38, L02807, doi:10.1029/2010GL046083, 2011.
Phillips, V. T. J., Andronache, C., Christner, B., Morris, C. E., Sands, D. C., Bansemer, A., Lauer, A., McNaughton, C., and Seman, C.: Potential impacts from biological aerosols on ensembles of continental clouds simulated numerically, Biogeosciences, 6, 987–1014, doi:10.5194/bg-6-987-2009, 2009.
Prenni, A. J., Demott, P. J., Rogers, D. C., Kreidenweis, S. M., McFarquhar, G. M., Zhang, G., and Poellot, M. R.: Ice nuclei characteristics from M-PACE and their relation to ice formation in clouds, Tellus B, 61, 436–448, 2009.
Pruppacher, H. R. and Klett, J. D.: Microphysics of Clouds and Precipitation, Kluwer Academic Publishers, Dordrecht, The Netherlands, 554 pp., 1997.
Radke, L. F., Hobbs, P. V., and Pinnons, J. E.: Observation of cloud condensation nuclei, sodium-containing particles, ice nuclei and the light-scattering coefficient near Barrow, Alaska, J. Appl. Meteorol., 15, 982–995, 1976.
Ramanathan, V., Crutzen, P. J., Kiehl, J. T., and Rosenfeld, D.:

Aerosols, climate, and the hydrological cycle, Science, 294, 2119–2124, 2001.

Rogers, D. C., DeMott, P. J., and Kreidenweis, S. M.: Airborne measurements of tropospheric ice-nucleating aerosol particles in the Arctic spring, J. Geophys. Res., 16, 15053–15063, 2001a.

Rogers, D. C., DeMott, P. J., Kreidenweis, S. M., and Chen, Y. L.: A continuous-flow diffusion chamber for airborne measurements of ice nuclei, J. Atmos. Ocean. Tech., 18, 725–741, 2001b.

Rosinski, J., Haagenson, P. L., Nagamoto, C. T., and Parungo, F.: Ice-forming nuclei of maritime origin, J. Aerosol. Sci., 17, 23–46, 1986.

Ross, S. M.: Stochastic Processes: Second Edition, Wiley Series in Probability and Mathematical Statistics, New York, NY, USA, Ch. 2, "The Poisson Process", 59–98, 1996.

Sander, R., Keene, W. C., Pszenny, A. A. P., Arimoto, R., Ayers, G. P., Baboukas, E., Cainey, J. M., Crutzen, P. J., Duce, R. A., Hönninger, G., Huebert, B. J., Maenhaut, W., Mihalopoulos, N., Turekian, V. C., and Van Dingenen, R.: Inorganic bromine in the marine boundary layer: a critical review, Atmos. Chem. Phys., 3, 1301–1336, doi:10.5194/acp-3-1301-2003, 2003.

Schnell, R. C.: Ice nuclei produced by laboratory cultured marine phytoplankton, Geophys. Res. Lett., 2, 500–502, 1975.

Schnell, R. C. and Vali, G.: Biogenic ice nuclei, 1. Terrestrial and marine sources, J. Atmos. Sci., 33, 1554–1564, 1976.

Sciare, J., Favez, O., Sarda-Esteve, R., Oikonomou, K., Cachier, H., and Kazan, V.: Long-term observations of carbonaceous aerosols in the Austral Ocean atmosphere: evidence of a biogenic marine organic source, J. Geophys. Res., 114, D15302, doi:10.1029/2009jd011998, 2009.

Seifert, M., Ström, J., Krejci, R., Minikin, A., Petzold, A., Gayet, J.-F., Schumann, U., and Ovarlez, J.: In-situ observations of aerosol particles remaining from evaporated cirrus crystals: Comparing clean and polluted air masses, Atmos. Chem. Phys., 3, 1037–1049, doi:10.5194/acp-3-1037-2003, 2003.

Shaffer, B. T. and Lighthart, B.: Survey of culturable airborne bacteria at four diverse locations in Oregon: urban, rural, forest, and coastal, Microb. Ecol., 34, 167–177, 1997.

Sorooshian, A., Padro, L. T., Nenes, A., Feingold, G., McComiskey, A., Hersey, S. P., Gates, H., Jonsson, H. H., Miller, S. D., Stephens, G. L., Flagan, R. C., and Seinfeld, J. H.: On the link between ocean biota emissions, aerosol, and maritime clouds: airborne, ground, and satellite measurements off the coast of California, Global Biogeochem. Cy., 23, GB4007, doi:10.1029/2009gb003464, 2009.

Stoermer, E. F. and Smol, J. P. (Eds.): The Diatoms: Applications for the Environmental and Earth Sciences, Cambridge University Press, Cambridge, 1999.

Ström, J., Seifert, M., Kärcher, B., Ovarlez, J., Minikin, A., Gayet, J.-F., Krejci, R., Petzold, A., Auriol, F., Haag, W., Busen, R., Schumann, U., and Hansson, H. C.: Cirrus cloud occurrence as function of ambient relative humidity: a comparison of observations obtained during the INCA experiment, Atmos. Chem. Phys., 3, 1807–1816, doi:10.5194/acp-3-1807-2003, 2003.

Tormo, R., Recio, D., Silva, I., and Munoz, A. F.: A quantitative investigation of airborne algae and lichen soredia obtained from pollen traps in South-West Spain, Eur. J. Phycol., 42, 248–252, 2001.

Twohy, C. H. and Anderson, J. R.: Droplet nuclei in non-precipitating clouds: composition and size matter, Environ. Res. Lett., 3, 045002, doi:10.1088/1748-9326/3/4/045002, 2008.

Twomey, S.: Pollution and planetary albedo, Atmos. Environ., 8, 1251–1256, 1974.

Twomey, S.: Aerosols, clouds and radiation, Atmos. Environ. A-Gen., 25, 2435–2442, 1991.

Vali, G.: Quantitative evaluation of experimental results on heterogeneous freezing nucleation of supercooled liquids, J. Atmos. Sci., 29, 402–409, 1971.

Vali, G.: Nucleation terminology, J. Aerosol Sci., 16, 575–576, 1985.

Vali, G.: Freezing rate due to heterogeneous nucleation, J. Atmos. Sci., 51, 1843–1856, 1994.

Vali, G.: Repeatability and randomness in heterogeneous freezing nucleation, Atmos. Chem. Phys., 8, 5017–5031, doi:10.5194/acp-8-5017-2008, 2008.

Verlinde, J., Harrington, J. Y., McFarquhar, G. M., Yannuzzi, V. T., Avramov, A., Greenberg, S., Johnson, N., Zhang, G., Poellot, M. R., Mather, J. H., Turner, D. D., Eloranta, E. W., Zak, B. D., Prenni, A. J., Daniel, J. S., Kok, G. L., Tobin, D. C., Holz, R., Sassen, K., Spangenberg, D., Minnis, P., Tooman, T. P., Ivey, M. D., Richardson, S. J., Bahrmann, C. P., Shupe, M., DeMott, P. J., Heymsfield, A. J., and Schofield, R.: The mixed-phase Arctic cloud experiment, B. Am. Meteorol. Soc., 42, 248–252, 2007.

Vogt, R., Crutzen, P. J., and Sander, R.: A mechanism for halogen release from sea-salt aerosol in the remote marine boundary layer, Nature, 383, 327–330, 1996.

Watson, S. W., Novitsky, T. J., Quinby, H. L., and Valois, F. W.: Determination of bacterial number and biomass in the marine environment, Appl. Enivron. Microb., 33, 940–946, 1977.

Wegener, A.: Thermodynamik der Atmosphäre, Johann Ambrosius Barth, Leipzig, 1911.

Welch, H. E., Muir, D. C. G., Billeck, B. N., Lockhart, W. L., Brunskill, G. J., Kling, H. J., Olson, M. P., and Lemoine, R. M.: Brown snow – a long-range transport event in the Canadian Arctic, Environ. Sci. Technol., 25, 280–286, 1991.

Wurl, O. and Holmes, M.: The gelatinous nature of the sea-surface microlayer, Mar. Chem., 110, 89–97, 2008.

Zhang, K. M., Knipping, E. M., Wexler, A. S., Bhave, P. V., and Tonnesen, G. S.: Size distribution of sea-salt emissions as a function of relative humidity, Atmos. Environ., 39, 3373–3379, 2005.

Zobrist, B., Koop, T., Luo, B. P., Marcolli, C., and Peter, T.: Heterogeneous ice nucleation rate coefficient of water droplets coated by a nonadecanol monolayer, J. Phys. Chem. A, 111, 2149–2155, 2007.

Zobrist, B., Marcolli, C., Peter, T., and Koop, T.: Heterogeneous ice nucleation in aqueous solutions: the role of water activity, J. Phys. Chem. A, 112, 3965–3975, 2008.